Kepes
http://scholopress.com/kepes-journal

2023 Volume 21 Issue 3 pp. 84-102

Computational Prediction of Spiropyrazoline Derivatives as Potential Acetylcholinesterase Inhibitors for Alzheimer's Disease Treatment

Moulay Ahfid El Alaouy [1], *Marwa Alaqarbeh [2], Salma El Bahi [1], Meryem Boutalaka [1], Soukaina Esslali [1, 4], Abdelouahid Sbai [1], Hamid Maghat [1], Farhate Guenoun [4], M'barek Choukrad [1], Tahar Lakhlifi [1], Mohammed Bouachrine [1, 3]

[1]Molecular Chemistry and Natural Substances Laboratory, Faculty of Science, University Moulay Ismail, Meknes, Morocco

[2]National Agricultural Research Center, Al-Baqa 19381, Jordan

[3]EST Khenifra, Sultan Moulay Sliman University, Benimellal, Morocco

[4]Laboratory of Chemistry-Biology Applied to the Environment, Chemistry Department, Faculty of Sciences, Moulay-Ismail University, B.P. 11201, Zitoune, Meknes, Morocco

Abstract

This work used computational methods of 3D-QSAR, molecular docking, ADMET, and molecular dynamics simulations to analyze the relationship between chemical structure and acetylcholinesterase inhibition mechanism by Spiropyrazoline derivatives. COMFA and COMSIA predicted the inhibitory activities of the proposed Spiropyrazoline derivatives against acetylcholinesterase, where the best models are (COMSIA/S + E + H) (Q^2 = 0.517, R^2 = 0.904, R^2 test = 0.931). Molecular docking results revealed that the new M1 complex interacts with critical residues in the major circuits of the AChE main chain, with residues TRP286, TRP86, TYR341, TYR72, TYR124, and TYR337 more than compound 2. This residue plays an essential role in the stability of the complex. A molecular dynamics simulation explored the binding stability and conformational interaction changes of M1 and molecule 2 with acetylcholinesterase complexes at 100 ns. Both compounds showed good stability regarding RMSD, Rg, RMSF, and SASA values. Compound M1 shows remarkable stability in the active site of AChE compared to compound 2. In addition, Lipinski's rule for predicting pharmacokinetics with ADMET is satisfactory. The retrosynthetic approach was used to develop an efficient and convenient synthetic route for preparing the target molecule M1.

Keywords: ADMET, Acetylcholinesterase inhibitors, Alzheimer's disease, 3D-QSAR, Molecular docking, Molecular dynamics simulation

1. Introduction

Alzheimer's disease (AD) is a complex neurodegenerative disorder characterized by various symptoms and is classified as one of the most prevalent forms of dementia. The primary causes of AD involve the abnormal aggregation of the protein amyloid-β, which forms plaques between neurons, and the excessive accumulation of tau protein tangles within neurons (Vyas et al., 2018). It is thought that amyloid plaques or their main parts, AB peptides, directly cause progressive neurodegeneration, which leads to complex cognitive changes caused by a biochemical and biophysical process (Kareti and Subash, 2020). Based on the research results, Alzheimer's

*Corresponding author

DOI https://doi.org/10.5281/zenodo.7936583#75

is considered an incurable disease, and early diagnosis contributes to slowing down the course of the disease by implementing specialized treatments(Long and Holtzman, 2019). The rapid growth of information regarding the molecular biology, pathophysiology, and prognosis of Alzheimer's disease has encouraged future prevention and treatment (De Strooper and Karran, 2016). According to previous studies, several compounds have been developed based on the "amyloid cascade" hypothesis as potential drugs for AD, including acetylcholinesterase (AChE) inhibitors and N-methyl-D-aspartate (NMDA) receptor antagonists that have been licensed for clinical use as memantine (Yao et al., 2022). Recently, several compounds have been developed that can treat or inhibit Alzheimer's disease by focusing on the genetic, environmental, and behavioral factors that play a role in the onset and progression of the disease (Tanenbaum and Lark, 2022). Therefore, pharmacological research in Alzheimer's disease focuses on inhibiting Acetylcholinesterase from restoring normal acetylcholine levels in the synaptic cleft (Dilshad et al., 2022). Spiroprozoline compounds possess high biological properties for treating several diseases, making them eligible as potential acetylcholinesterase inhibitors that should be investigated for their pharmacokinetic efficacy properties.
Computational techniques based on theoretical mathematics and chemical informatics has been widely used to discover and design new drug candidates over the past two decades. Quantitative structure-activity relationships (QSARs) are computational statistical models that reveal relationships between chemical compound structural properties and biological activities(Yu et al., 2023). Molecular docking is widely used to provide details of protein-ligand interactions, allowing 3D information graphs for a deeper understanding of the molecular binding pattern(Khedkar et al., 2010a). Molecular dynamics simulation examines the stability of the molecule-protein complex by calculating the potential energy function and atomic force and solving the equation using Newton second law (Rapaport et al., 1996). The main objective of this research is to investigate the therapeutic activity properties of previously synthesized 20 spiropyrazoline compounds by Gutti et al. as AChE inhibitors, where the synthesis route shown in **Fig. 1** (Gutti et al., 2019). QSAR studies yielded predictive models and a series of visual contour maps. Then, molecular docking studies were done to determine the binding affinity and show how the target molecules and proteins interacted. An ADMET predictor was essential for the efficacy and safety of the therapeutic agent. In addition, MD studies were performed to validate the results of all modeling methods by comparing the stability of the protein-molecule complex system.

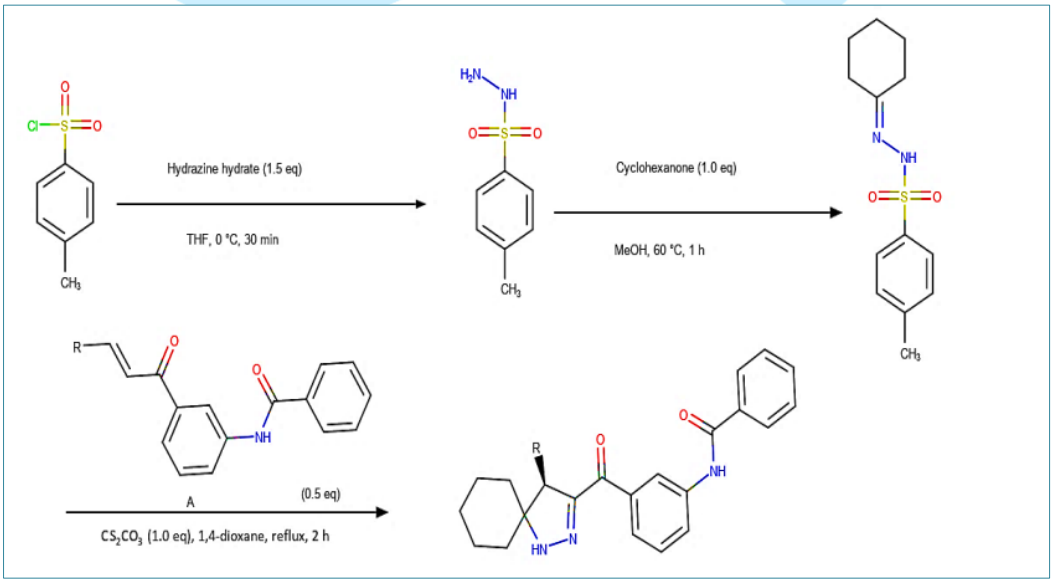

Fig. 1 synthesis of spiropyrazoline derivatives

Finally, retrosynthesis is an essential tool in organic chemistry, used to retroactively synthesize routes for a target molecule by breaking them down into simpler reaction steps. It offers numerous advantages, such as the rational design of synthetic routes, optimization of chemical production, exploration of new strategies,

and assessment of the feasibility of syntheses. Chemists can develop coherent and efficient reaction sequences using retrosynthesis, saving time and resources. It also fosters innovation by encouraging the exploration of new synthetic interactions and methodologies. The current study provides theoretical information for developing, predicting and designing new compounds that specifically target acetylcholinesterase.

2. Materials and method

2.1 Data set preparation and division

This work used twenty spiroparazoline compounds synthesized by Guti et al., to investigate acetylcholinesterase inhibitory activity. They divided into two groups: 75% of them (15 compounds) were used to develop the QSAR model, while the remaining compounds 25% (5 compounds) were used to validate the external model. **Fig. 1 and Table 1** show the structures of the 20 compounds of spiroparazoline and their activity levels.

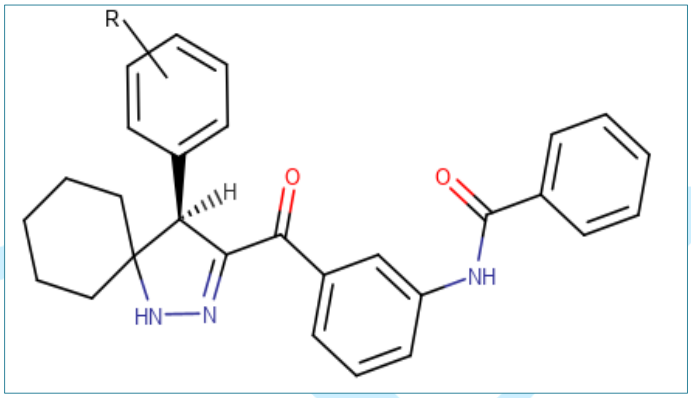

Fig. 2 The formula of the studied spiropyrazoline derivatives

Table 1 Activities and structures of spiropyrazoline derivatives

N°	R	IC_{50} (µM)	pIC_{50}
1*	H	1.973	5.713
2	4-Cl	0.464	6.333
3	2-Cl	1.967	5.706
4	2.4-diCl	1.327	5.877
5	4-Br	1.139	5.943
6	3-Br	1.77	5.752
7*	4-F	0.948	6.023
8	3-F	1.627	5.788
9*	4-OMe	2.319	5.634
10	3-OMe	2.831	5.548
11	3.4-diOMe	3.011	5.521
12	4-CF_3	1.453	5.836
13	3-CF_3	1.921	5.716
14	4-OCF_3	2.24	5.65
15	4-CN	1.78	5.75
16	3-CN	1.962	5.707
17*	4-Me	4.686	5.33
18	2-Me	5.883	5.23
19	4-iPr	7.145	5.146
20*	α-Napthyl	29.19	4.535

*Test set molecules

2.2 Molecular superposition

Molecular superposition is crucial in building a stable and reliable QSAR model. In this work, the model of compound 2 had the highest inhibitory effect, and the compounds in the training and test sets were superimposed using the Align database of Sybyl software based on their standard structure **(Fig. 1 and Fig. 2)** shows an overlay of 20 spiropyrazoline derivatives (Yu et al., 2022).

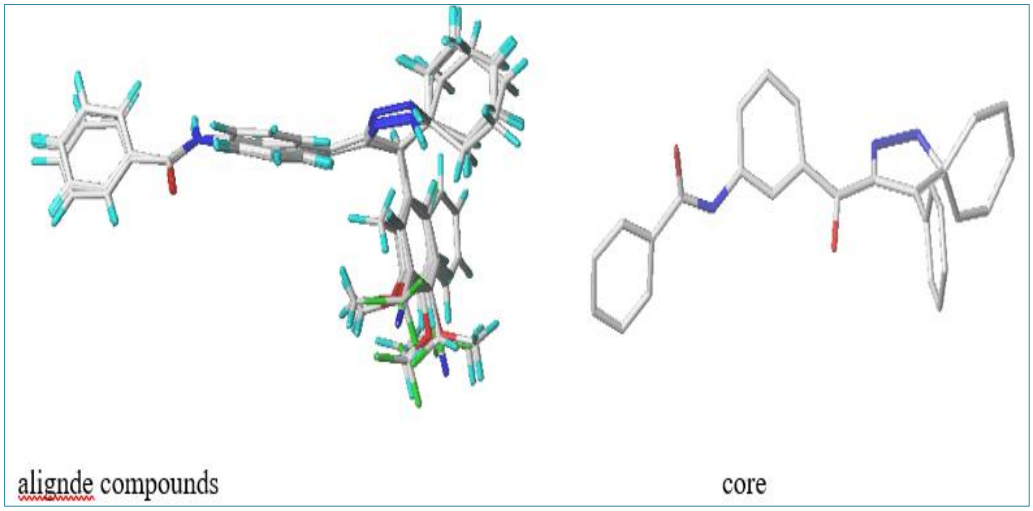

Fig. 3 Core (right) and aligned molecules (left) using Molecule 2 as a model

2.3 CoMFA and CoMSIA studies

One of the most important 3D-QSAR method results is the study of ligand-receptor interaction's local physical and chemical properties(Rose et al., 2018). A 3D cubic mesh was developed with a grid spacing of 1 Å and 4 Å and a distance-dependent insulator at each mesh site. CoMFA fields were calculated using a sp^3 carbon probe with +1 charge to calculate steric field energies and electrostatic fields. CoMSIA calculates similarity indices in the space around each of the molecules in the dataset that have already been aligned using certain methods. CoMSIA uses a Gaussian-like distance dependence function between the probe and the atoms of the molecules to avoid singularities at atomic locations and excessive fluctuations in potential energy for.

2.4 Partial least square (PLS) statistical analysis

CoMFA and CoMSIA models were analyzed using the PLS method. A cross-validation study was performed using a single approach (LOO) to determine the optimal number of components (ONC) and the cross-validation coefficient of determination Q2(Srivastava et al., 2010). Then, 3D-QSAR models were generated by non-cross-validation, in which the correlation coefficient (R2), F values (F), and standard error of estimation (SEE) were calculated(Li et al., 2013). Parameters derived from previous PLS studies can be used to assess predictive performance and predict activity for molecules in the test set.

2.5 Molecular docking

Protein-ligand docking is often used to predict how the structures of ligands and receptors will interact by finding binding modes that are energetically favorable. Since a cubic box usually represents the binding region and center are essential for correct docking because they define the spatial boundary of the corresponding sample (Liu et al., 2020).

In this work, the web server http://cao.labshare.cn/cb-dock/ was used to prepare a protein file in PDB format and ligand files in MOL2, MOL, or SDF formats as input. After receiving input files, CB-Dock converts OpenBabel to pdbqt format (O'Boyle et al., 2011).Then, CB-Dock is used to predict the protein's cavities, and the centers and diameters of the N most important cavities (n = 5 by default) are found. During the docking process, AutoDock Vina performs a series of calculations and simulations to explore the potential binding

modes of the ligands to the target protein. The number of rounds denoted as N, determines the depth and thoroughness of the search. A higher value of N typically leads to a more exhaustive exploration of binding modes. Upon completion of the specified number of rounds, AutoDock Vina generates the final results. These results usually include the predicted binding affinities and the corresponding binding poses for each ligand. The binding affinities estimate the strength of interaction between the ligands and the protein, while the binding poses illustrate the spatial arrangement of the ligand within the protein's active site. These results serve as valuable insights for further analysis and decision-making in drug discovery (Rose et al., 2018).

2.6 ADMET and drug-likeness prediction

The first clinical trial is an essential part of drug research and development because it checks for pharmacokinetic properties and prevents late-stage failures from happening. Most clinical studies failed because absorption, distribution, metabolism, elimination, and toxicity (ADMET) properties were not calculated as needed to determine how well a drug works and its safety. Swissadmet (Daina et al., 2017) and pkCSM(Pires et al., 2015) were used to predict ADMET. According to Lipinski's criteria, these two strategies significantly reduce the risk of drug development failure, where oral bioavailability is high when the proposed molecule follows the Lipinski criteria(Daina et al., 2017) .To be considered orally bioavailable, a molecule must have a molecular weight of 500 DA, logP of 5, hydrogen bond donors (DBL) of 5, hydrogen bond acceptors (HBA) of 10, and a topological polar surface area (TPS) of 140.

2.7 MD Simulations

MD simulations are widely used in gathering information about protein and ligand dynamics. NAMD 2.13 software performed MD simulations of the moored complexes (Ponce et al., 2021).For MD modeling, compounds with the best binding affinity were studied further. In this study, the formation of protein-ligand complexes was looked at, which led to more proof that the docking results were correct. Then, using TIP3P as a solvent, they were reduced to a minimum (Phillips et al., 2005).After neutralizing the entire system, counters (Na^+) were added to reduce it. The periodic boundary conditions were generated using the 97.77, 97.86, and 97.47 dimensions in x, y, and z, respectively. The parameters for the best docking results were generated using the general CHARMM force field(Khalil et al., 2022). The canonical set (NVT) was used for equilibration, while the isobaric set for construction (NPT) was used. The pressure was adjusted to 1 atm using a Langevin Nose'-Hoover barostat piston for an MD efficiency of 100 ns (Nosé, 1984), with a period of 0.1 ps and a Langevin piston decay of 0.05 ps. The temperature was set to 298.15 K using a Langevin thermostat (Grest and Kremer, 1986).

2.8 Retrosynthesis method

ASKCOS (Automated System for Knowledge-based Continuous Organic Synthesis) is an open-source website (https://askcos.mit.edu/) for the retrosynthesis planning using the SMILES of the compounds (Shen et al., 2021). This program contains various modules for planning a retrosynthesis as the one-step retrosynthesis module provides direct precursors of the M1 target molecule in a complete synthesis pathway(Coley et al., 2019), while the tree-building module that automatically generates a multi-step retrosynthesis.

3. Results and discussion

3.1 CoMFA analysis

Table 2 shows the results of the CoMFA model. Based on PLS analysis, the CoMFA (S + E) field has a more substantial influence on activities than electrostatic (E) and steric (S) fields, as validated by a Q^2 value of 0.544 and correlation coefficient (R^2) of 0.947. F value of 32.473, a standardized error (SEE) of 0.087, and 5 as the

optimum number of components. With an R^2test value of 0.53, the molecules in the test set also prove that the CoMFA (S+E) model is correct.

Table 2 Possible CoMFA results

	Q^2	N	SEE	R^2	F	R^2 Test
Steric (S)	0.642	2	0.068	0.963	46.254	0.48
Electrostatic (E)	-0.074	2	0.066	0.964	48.535	0.524
S + E	**0.544**	**5**	**0.087**	**0.947**	**32.473**	**0.53**

3.2 CoMSIA analysis

Eighteen models were selected based on statistical parameter values throughout the construction process. The results of the different combinations of five variables used to build the different CoMSIA models are shown in **Table 3.** In the model (COMSIA/S+E+H), the three different fields: steric (S), electrostatic (E) and hydrophobic (H), show the best model (Q^2 = 0.517; R^2 = 0.904; F = 16.957; SEE = 0.109; ONC = 3). The molecules in the test set also verified this model with R^2test = 0.9314, showing that this model is efficient and predictive compared to the other models. The contributions of the steric, hydrophobic, and electrostatic fields were 22.5%, 28.3%, and 49.1%, respectively, indicating that the electrostatic, steric, and hydrophobic fields played a key role in this model. Finally, since the model (COMSIA/S+E+H) had a higher Q^2 and R^2 than the CoMFA (S+E) model, it was the most appropriate and would provide the most statistical keys in this research.

Table 3 Possibilities of combining (COMSIA) fields

	Q^2	N	SEE	R^2	F	R^2 Test
S+H	0.551	4	0.122	0.879	13.106	0.522
S+E+H	**0.517**	**3**	**0.109**	**0.904**	**16.957**	**0.9314**
S+E+H+A	0.517	3	0.117	0.89	14.396	0.92
S+E+D+A	0.535	4	0.12	0.884	13.693	0.64
H+A	0.622	2	0.132	0.857	10.83	0.19
S+E+D+H	0.624	3	0.110	0.901	16.378	0.878
E+D+A+H	0.512	3	0.116	0.891	14.789	0.731
S+E+D+A+H	0.613	3	0.107	0.907	17.495	0.889
D+A	0.557	4	0.181	0.73	4.95	0.747
D+A+H	0.614	2	0.131	0.86	11.19	0. 28
H	0.638	5	0.13	0.29	11.328	0.29
S+A	0.56	4	0.159	0.796	7.016	0.38
H+D	0.649	5	0.12	0.884	13.671	0.623
E	0.141	3	0.183	0.727	4.802	0.65
S	0.497	3	0.163	0.78	6.545	0.583
D	0.578	2	0.189	0.71	4.40	0.37
S+H+D	0.682	2	0.122	0.879	13.13	0.48
A	0.537	4	0.190	0.708	4.356	0.673

The actual and predicted activities of the $\mathrm{CoMFA/S+E}$ and COMSIA/S+E+H, models of AChE inhibitors are shown in (**Table 4**).

Table 4 Experimental and predicted PIC_{50} of the CoMFA/$S + E$ and CoMSIA/$S + E + H$ models

N	pIC_{50} (M)	$CoMFA/S + E$		$COMSIA/S + E + H$	
		Predicted	*residuals*	*Predicted*	*Residuals*
1*	5.713	5.865	-0.152	5.894	-0.181
2	6.333	6.174	0.159	6.099	0.234
3	5.706	5.683	0.023	5.687	0.019
4	5.877	5.948	-0.071	5.894	-0.017
5	5.943	6.041	-0.098	6.137	-0.194
6	5.752	5.753	-0.001	5.804	-0.052
7*	6.023	6.07	-0.047	6.052	-0.029
8	5.788	5.811	-0.023	5.81	-0.022
9*	5.634	6.294	-0.66	5.987	-0.353
10	5.548	5.488	0.06	5.511	0.037
11	5.521	5.501	0.02	5.48	0.041
12	5.836	5.79	0.046	5.837	-0.001
13	5.716	5.764	-0.048	5.696	0.02
14	5.65	5.673	-0.023	5.615	0.035
15	5.75	5.794	-0.044	5.749	0.001
16	5.707	5.708	-0.001	5.748	-0.041
17*	5.33	6.004	-0.674	5.884	-0.554
18	5.23	5.173	0.057	5.294	-0.064
19	5.146	5.201	-0.055	5.143	0.003
20*	4.535	5.601	-1.066	5.565	-1.03

*Test set

3.3 Y-randomization test of model

A randomization test was done to eliminate random associations and prove that the model (COMSIA/S + E + H) was correct. As shown in (**Table 5)** the model (COMSIA/S + E + H) has lower Q^2 and R^2 values than the prototypes after this test, indicating that the original model was not randomly generated.

Table 5 R^2 train and Q^2 LOO values after the Y-randomization experiments

Model	R	R^2	Q^2
Original	**0.844**	**0.712**	**0.556**
Random 1	0.254	0.064	-0.618
Random 2	0.455	0.207	-0.304
Random 3	0.185	0.034	-1.348
Random 4	0.297	0.088	-0.641
Random 5	0.288	0.082	-0.601
Random 6	0.538	0.290	-0.36
Random 7	0.594	0.353	-0.27
Random 8	0.427	0.183	-0.301
Random 9	0.285	0.081	-0.948
Random 10	0.184	0.034	-1.106
Random Models Parameters			
Average	0.3512	0.1420	-0.650

3.4 Interpretation of model CoMSIA contour.

The field contour map of the selected model (COMSIA/S+E+H) is shown in (**Fig. 4),** where the steric field, hydrophobic field, and electrostatic field distributions of CoMSIA are shown in (**Fig a, b, and c**). The steric field (a): The green and yellow hues suggest that the bulky group is beneficial for boosting activity and unfavorable for decreasing activity, respectively. The green contour obtained near *the para*-R substituent indicates that adding bulky substituents could increase biochemical activity in this position. Also, it explains the higher activity of compound 9 with the -OMe radical in para position compared to compound 17 with the -Me radical in the same position. In addition, the *para* position is more efficient than *meta* or *ortho* positions, which explains the higher activity of compound 12 with the $-CF_3$ radical compared to compound 13 with the same radical in the *meta* position. For the hydrophobic contour map (b) of (COMSIA/S+E+H), yellow contours represent favored hydrophobic regions, as shown around *para* radical R position in (**Fig. 4b),** while white contours represent favored hydrophilic regions (Zeng et al., 2013). In the electrostatic field (c), blue contours (80% contribution) represent places where positive electrostatics are favored, while red contours (20% contribution) represent places where negative electrostatics are favored. (**Fig. 4c)**. A red color outline is close to the *para*-R substitution position, indicating that introducing highly electronegative groups or atoms can increase their biochemical activity. As illustrated, compound 2 has -Cl atom at *para* position with higher activity than compound 5, which has -Br atom at the same position.

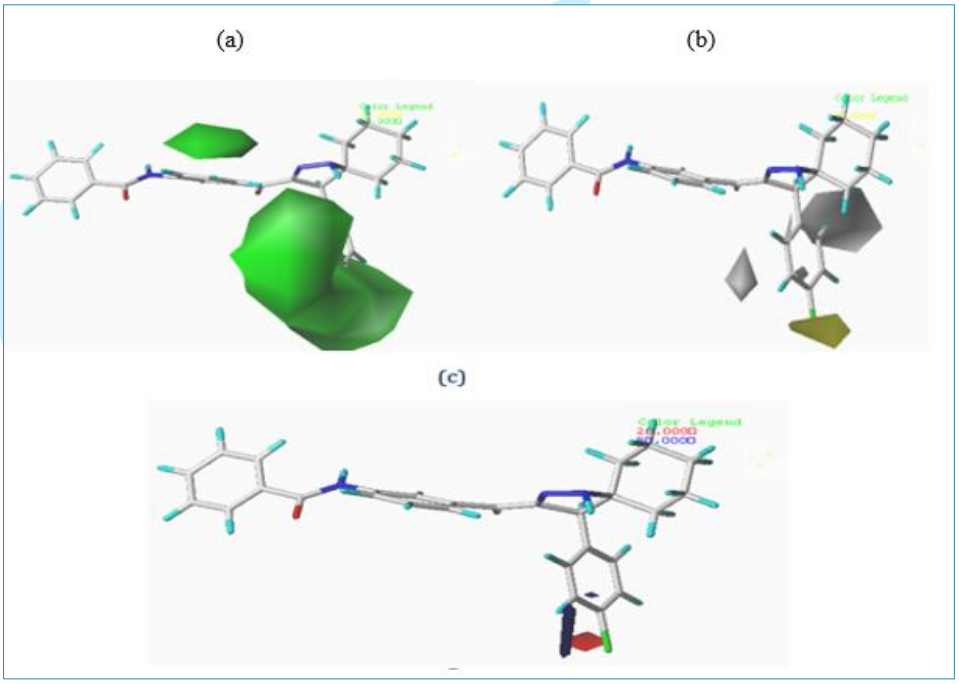

Fig. 4 CoMSIA model contour map results. (a) Steric field, (b) hydrophobic field, (c) electrostatic fields

3.5 Newly designed compounds

In this work, the main factors influencing the inhibitory activity were determined, and the substituents were fitted in the appropriate zones using contour maps for the best model (COMSIA/S+E+H) to predict the activity of the newly developed compounds as shown in (**Table 6**) (Meng et al., 2020).

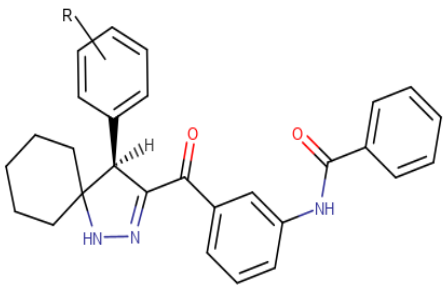

Table 6 Anticipate new designs and their activities through the (COMSIA/S+E+H) model

N	R	pIC_{50}(Pred) (COMSIA/SEH)
2	4-Cl	6.099
M1	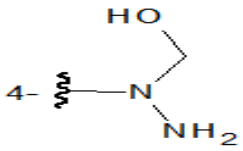	6.304
M2	4-Me ,3-F	6.306
M3	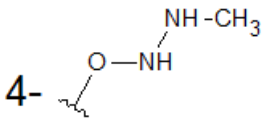	6.303
M4	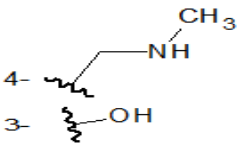	6.303
M5	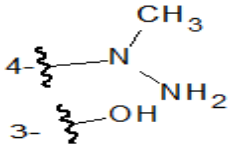	6.302
M6	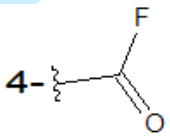	6.302
M7	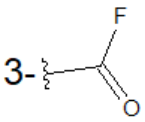	6.298

3.6 Analysis of drug-likeness and in-silico ADMET prediction

ADMET and drug propensity measurements were used to confirm that the proposed compounds could be used as drugs. This technique usually applies to molecules selected for high-quality drug similarities. **Table 7** shows ADMET values for all expected spiropyrazoline derivatives since all the results were within a reasonable range**.** Also, ADMET properties affect potential drugs pharmacokinetics (absorption, distribution, metabolism, and excretion) and pharmacodynamics (drug effectiveness and toxicity)(Islam et al., 2021). All proposed molecules listed in **Table 7** do not exceed the 500 DA threshold, and the toxicity and permeability data in the table show that the proposed molecules M1, M2, M3, M4, M5, M6, and M7 are not toxic and do not cross the BBB. Drugs with adequate M.R. and nRotband values show proper intestinal absorption and oral bioavailability.

Table 7 Lipinski properties of new spiropyrazoline derivatives, Analyzed with SwissADMET

	M.W. (≤500Da	LogP (<5)	nHBD (≤5)	nHBA (≤10)	TPSA (<140 Å^2)	Drug-likeness Lipinski	CYP3A4 inhibition	CYP3A4 substrate	M.R.	Log Kp S/N (cm/s)	Log S	nRotB	AMES toxicity
M1	497.59	4.197	4	7	120.05	YES	YES	YES	151.79	-6.28	-5.47	7	NO
M2	497.56	5.985	2	5	87.63	YES	YES	YES	148.93	-5.17	-6.51	6	NO
M3	497.59	4.585	4	7	103.85	YES	YES	YES	150.62	-5.78	-5.85	8	NO
M4	496.61	4.99	4	6	102.82	YES	YES	YES	153.12	-5.72	-5.95	7	NO
M5	497.59	4.583	4	7	120.05	YES	YES	YES	152.65	5.73	-6.02	6	NO
M6	483.53	5.677	2	5	87.63	YES	YES	YES	143.96	-5.35	-6.20	6	NO
M7	483.53	5.677	2	5	87.63	YES	YES	YES	143.96	-5.35	-6.2	6	NO

3.7 Docking results

Before running docking simulations, the co-crystal structures were examined using the Atlas of Protein Communications (http://www.mrc-lmb.cam.ac.uk/pca) to identify amino acids of interest and their chemical properties. An innovative interaction analysis technique, the asteroid diagram, takes advantage of a multi-level representation of non-covalent interactions. From **Fig. 5A**, the first shell residues, such as TRP286, TRP86, TYR341, TYR72, TYR124, and TYR337, contributed more to the receptor-binding interactions. These data show which residues are involved in the interactions between receptors and ligands. The thickness of the blue matrices in **Fig. 5B** also shows how many atomic contacts there are. These results provided us with the baseline data we needed to assess the interaction patterns of the investigated compounds**.**

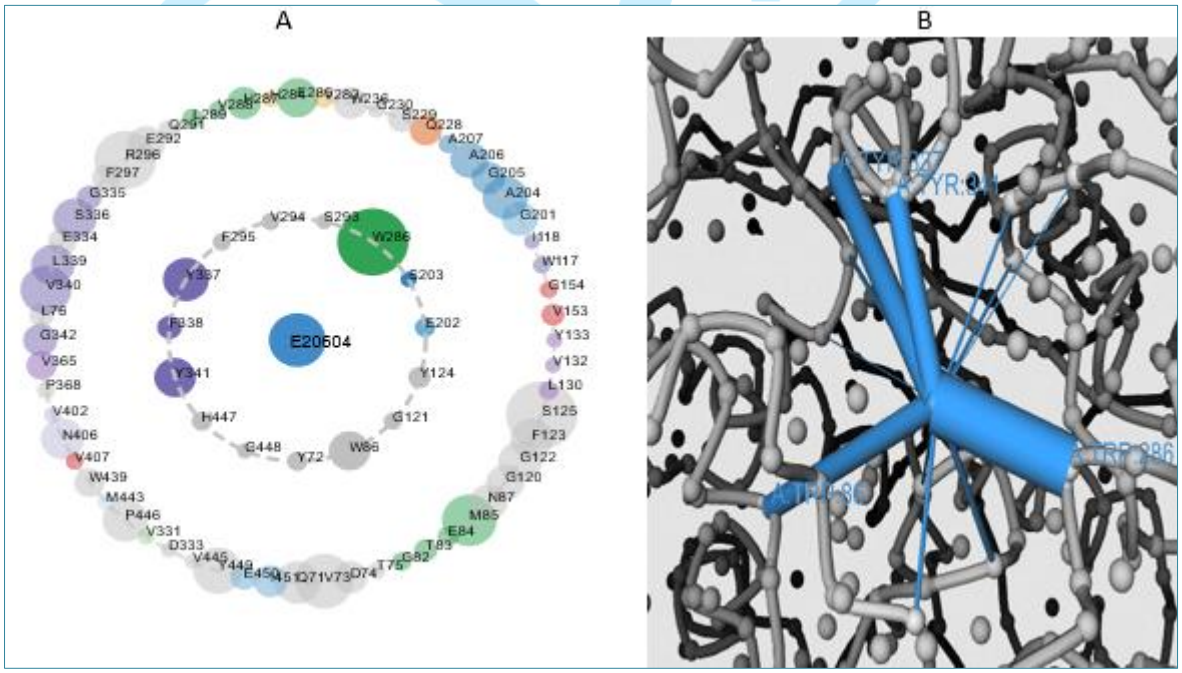

Fig. 5 Asteroid graph and network view of protein-ligand interactions

For model validation (COMSIA/S + E + H) of the 3D QSAR technique, molecular docking provides insights into potential interactions between ligand derivatives and receptors. The reliability of docking can be verified by re-docking, which is useful for assessing the reliability and accuracy of docking algorithms. We begin by downloading acetylcholinesterase (PDB: 4EY7), from the RSCB protein database using the URL (https://www.rcsb.org/). Recombination reliability is measured by the RMSD value, which is 0.56 Å < 2Å, indicating which protein site used is the most active. **Fig. 6** shows the relationship between the crystalline and stable forms of the binder.

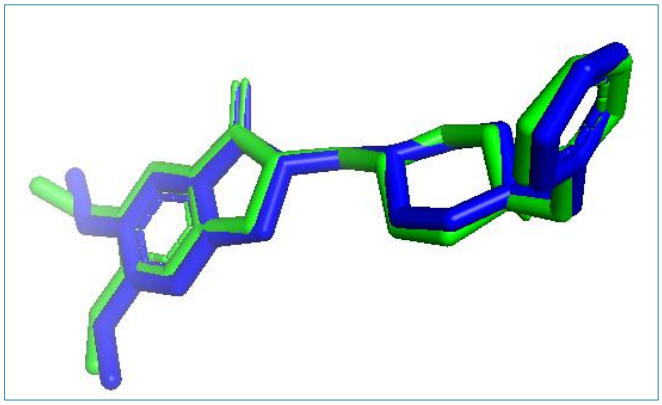

Fig. 6 Re-docking pose (blue: Original, green: Docked), the RMSD value is 0.56 Å

The results in **Fig.7 and 8** show molecular docking interaction modes between the acetylcholinesterase receptor (PDB: 4EY7), the most active molecule 2, and the proposed compound M1. The results of the docking study presented in **(Fig. 7)** show that chemical molecule 2 exhibits conventional hydrogen bonding interactions with residues TYR: 124 and TYR: 72, a pi-pi stacking interaction with residues TYR: 337, PHE: 338 and TYR: 341, Pi-alkyl interactions with residues LEU: 289 and TRP: 447, an attractive charge reaction with residue TRP: 286 and Pi-Anion interaction with residue ASP: 74. The presence of these interactions increases the biochemical efficiency of acetylcholinesterase inhibitors. Using CB-DOCK software, the docking score was -11.5 kcal/mol (Ali Mohammed Al-Ahmed, 2022).

The interactions of the complex (compound M1-AChE) were shown in **Fig. 8**, with residues TYR:72 and GLU:71 interacting in a typical way through hydrogen bonds. Pi-pi stacked interactions with residues TRP:286, TYR:341; TYR:124. A carbon-hydrogen bonding interaction with residue TRP:86; a Pi donor hydrogen bonding interaction with residue TYR:124; followed by two Pi-alkyl interactions with residues TRP:86 and HIS:447; and Pi-sigma interaction with residue TRP:86. The docking score was -11.8 kcal/mol, better than that of compound 2 because compound M1 formed stronger interactions with AChE residues. The key residues obtained in the docking results reported above were consistent with the critical residues in the large circles on the main chain of AChE. These results confirmed the stability of the M1 complex in the active pocket and showed stronger inhibitory activity against the AChE enzyme than molecule 2 (El-Assaly et al., 2021). The results indicated that compound M1 has greater stability in the active site of the acetylcholinesterase enzyme than molecule 2. Finally, all these results are supported by 3D-QSAR analysis, demonstrating that the newly synthesized spiroperazole derivatives are stable and more potent than the actual drug (molecule 2).

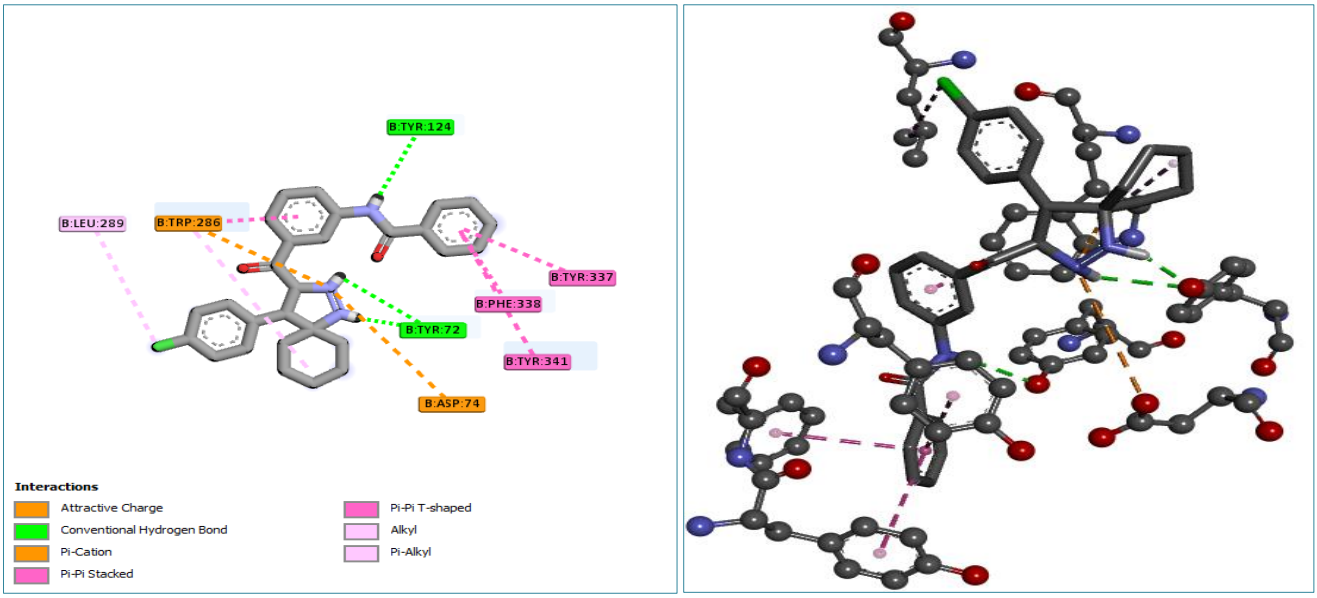

Fig. 7 Representation of chemical interactions of 2 compounds at receptor binding sites in 2D and 3D docking

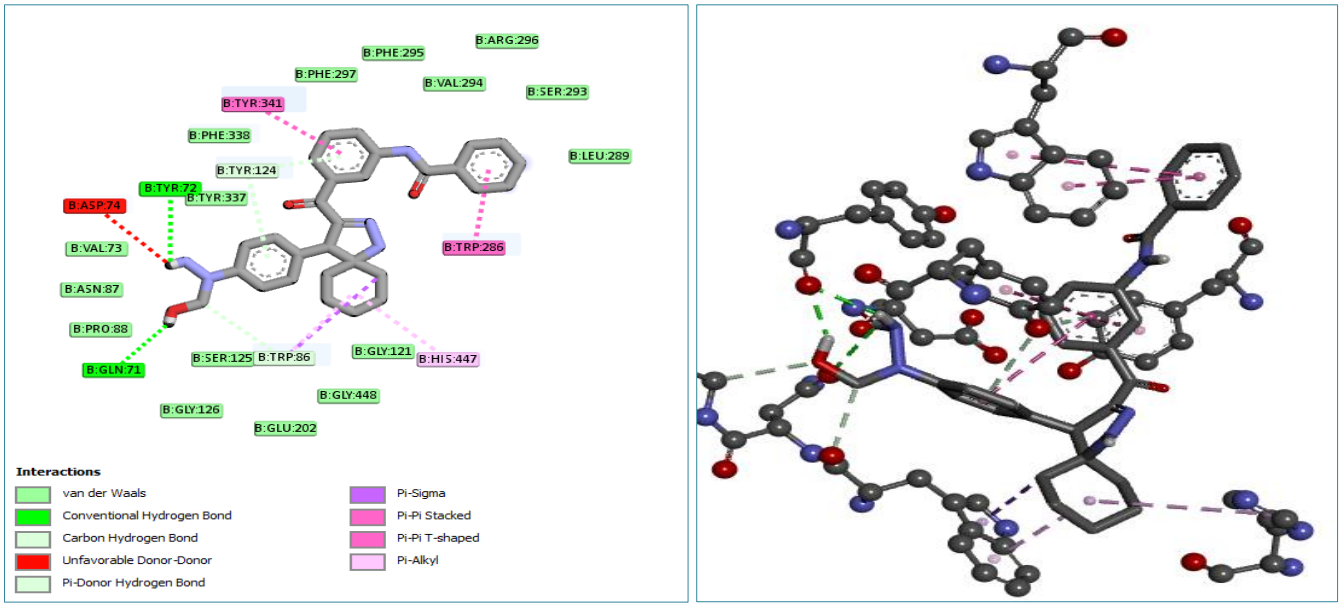

Fig. 8 Representation of chemical interactions of M_1 compounds at receptor binding sites in 2D and 3D docking

3.8 Molecular Dynamics simulation

RMSD (root mean square deviation) is the average variation in the location of atoms between two stacked structures. In reality, the deviation is determined by the location of the atoms in the Cα or main chain. The RMSD values of the most active compound 2 **(Fig. 9A)** increased from 2.1 A˚ in the initial 44 ns and maintained equilibrium at 1.8 after 44 ns of the process. However, the protein-ligand complex was stable for 100 ns with an RMSD of less than 2.3 Å, whereas the RMSD of the protein was less than 1.8 Å during the simulation period. The designed molecule **M_1 (Fig. 9B)** increased by about 2.5 A˚ in the initial 17 ns and maintained equilibrium at about 2.1 after 17 ns of treatment. However, protein-ligand complex was stable for 100 ns with an RMSD less than 2.6 Å. Moreover, the RMSD trajectory of the protein was stable throughout the simulations with an RMSD less than 1.9 Å.

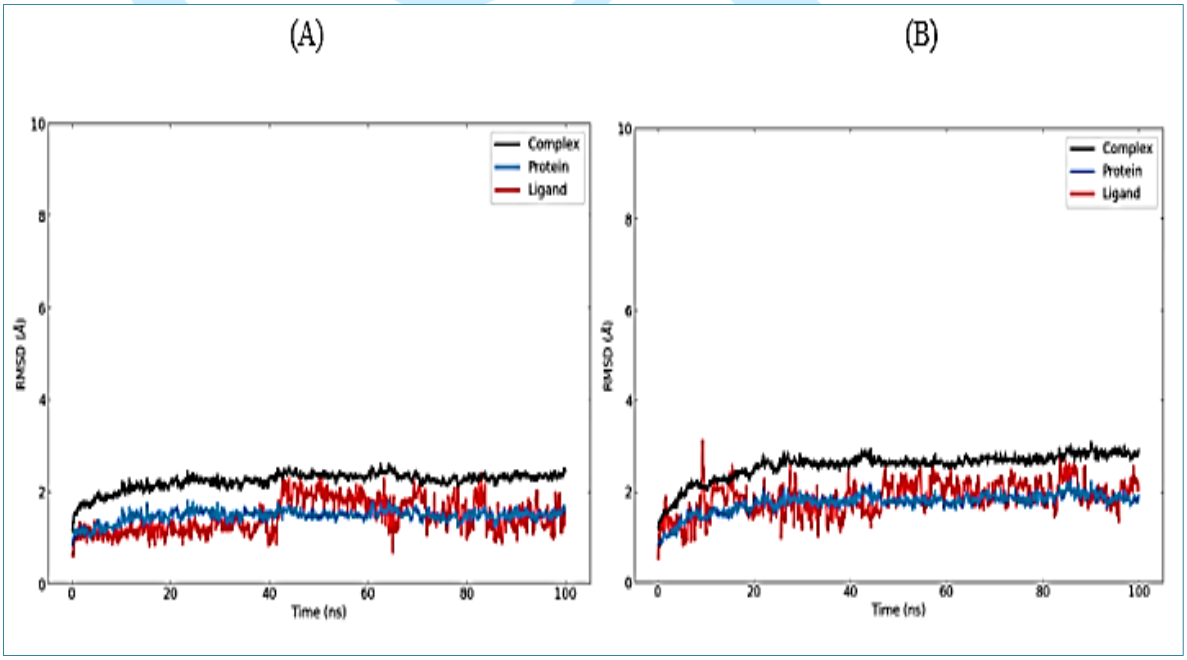

Fig. 9 RMSD of active molecule 2 (A) and designed molecule M_1 (B) with protein

Root means square variability (RMSF) determines local protein chain changes. Three significant fluctuations of 3.4 Å, 3.1 Å, and 2.58 Å appear in the loop region of residues 535, 98, and 264, respectively, for active Acetylcholinesterase (AChE)-molecule 2 complex **(Fig. 10C).** Maximum fluctuations of 3.9 Å, 3.7 Å, 2.9 Å, and

3.5 Å also appear in the loop region of residues 96, 265, 96, 430, and 535, respectively, in protein- M_1 molecule complex **(Fig. 10D).** Moreover, in both complexes, most protein residues have RMSF values of less than 1.7 Å, which means that these ligands are not subject to significant conformational changes over time. In general, both complexes fluctuate in approximately the same manner (Liu et al., 2022).

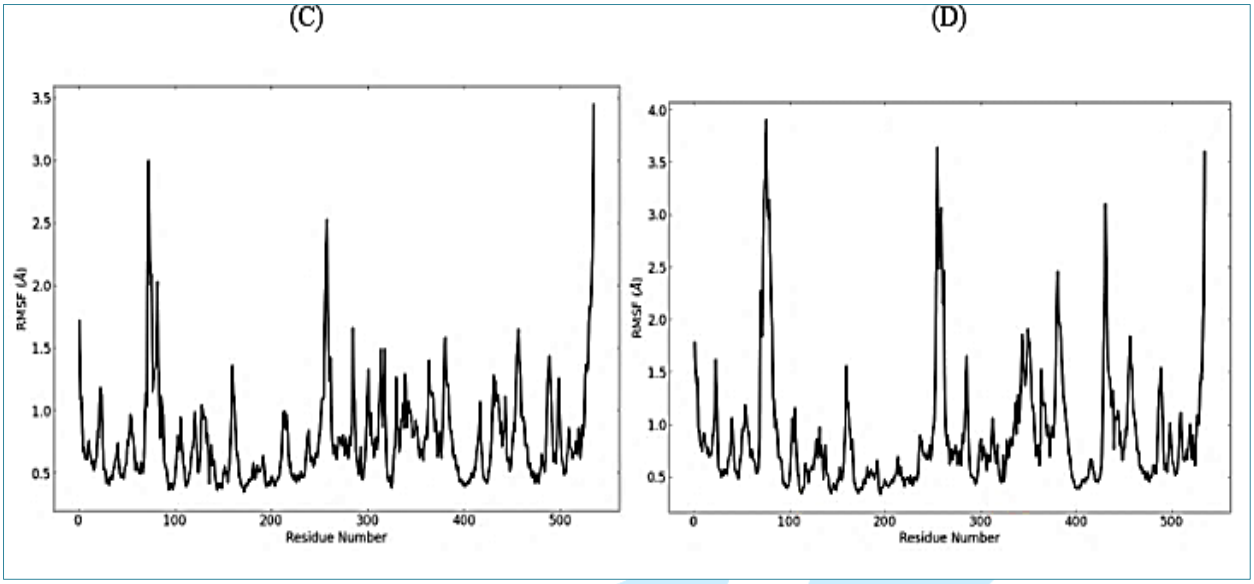

Fig. 10 RMSF of the active molecule complex 2 (C) and the proposed molecule complex M_1 (D) with the AChE

The radius of gyration (Rg) uses to assess the compactness of proteins. When the radius of gyration is large, the protein is considered stretched; when it is small, the protein folded. This variable can help highlight the balance between stretching and folding. The Rg value indicates the degree of compactness of the protein. Also, the Rg value indicates the degree of compactness of the protein. The higher the value, the lower the coherence of the protein.

Starting at 32 ns, the average Rg values for molecular complex 2 **(Fig. 11E)** and molecular complex M_1 **(Fig. 11F**) were 23. 35 Å and 23.3 Å, respectively. Despite some fluctuations due to the dynamic nature of AChE, all systems show consistent values throughout the simulations. In addition, it appears that both complexes were slightly more compact.

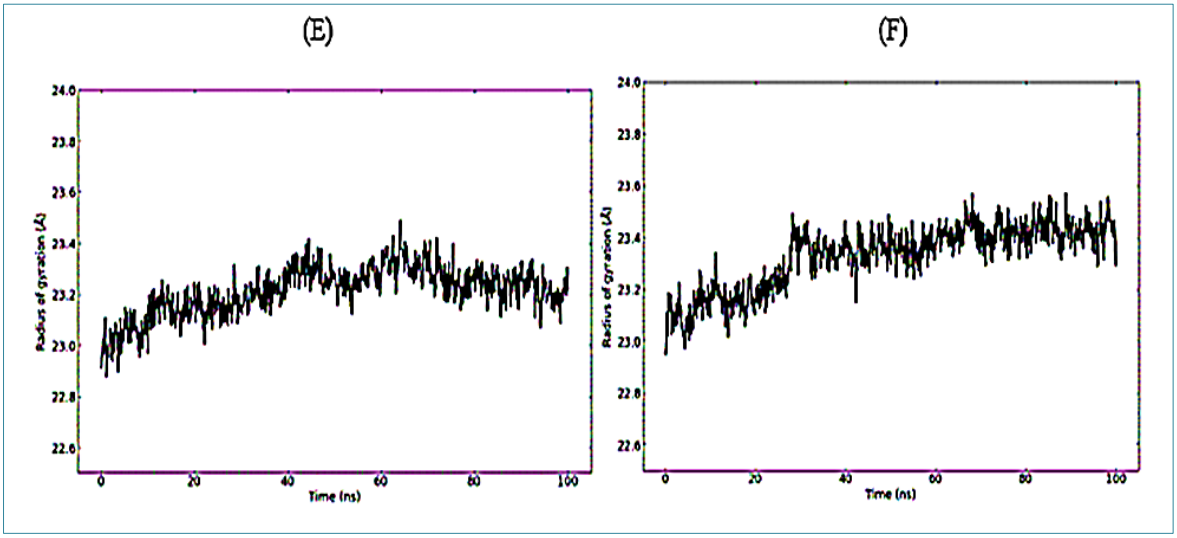

Fig. 11 Rg of the active molecule complex 2 (E) and the designed molecule complex M_1 (F)

Solvent-accessible surface area (SASA) is another important metric for figuring out how much of the protein's surface can interact with other molecules and particles of the solvent (Khedkar et al., 2010c). (SASA) for molecular complex 2 shown in (**Fig. 12 (A)),** it increased by 21963.986 A˚ in 17 ns of departure. It maintained

equilibrium until 41 ns and, after a fluctuation of 22724.068 A˚ in 66 ns, remained stable until 69 ns, then decreased by about 22550 A˚ in 75 ns, and maintained equilibrium until the end of the simulation. For the proposed molecular complex M1 shown in **(Fig. 12 (B))**, the SASA values gradually increased to about 23499.77 A˚ in the initial 45 ns and maintained equilibrium during the simulation. In the AChE active site, the complex of the proposed molecular structure by AChE has excellent stability.

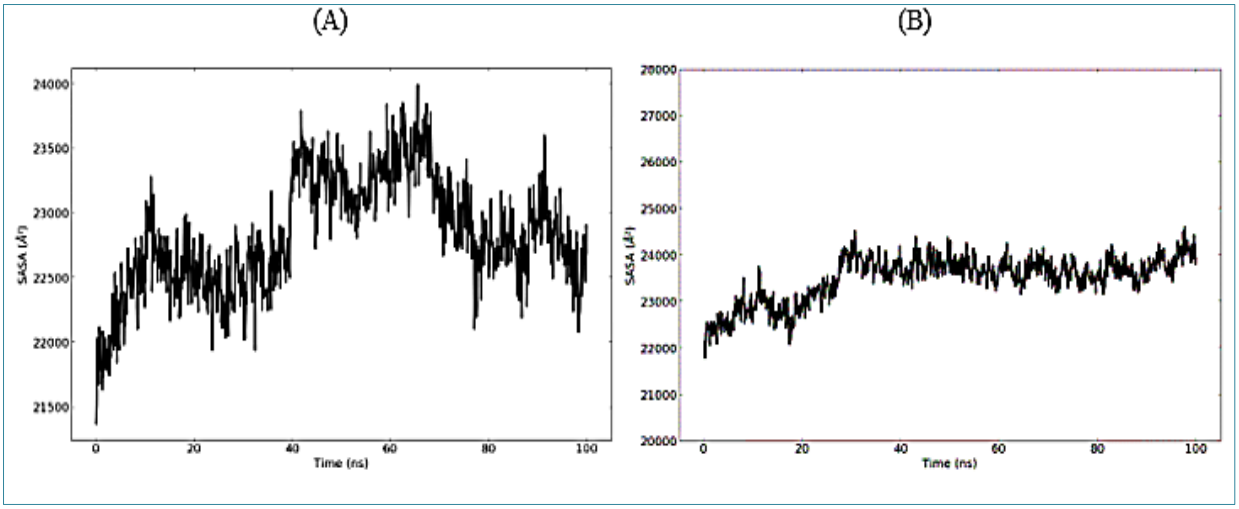

Fig. 12 (SASA) for the active molecular complex 2(A). proposed molecular complex M_1(B)

Hydrogen bonding is essential in the ligand-receptor interaction, with the protein preferring to create more hydrogen bonds with the M1 design molecule **(Fig. 13F**) than with molecule 2, as shown in **(Fig. 13E),** corroborating the results of the docking research.

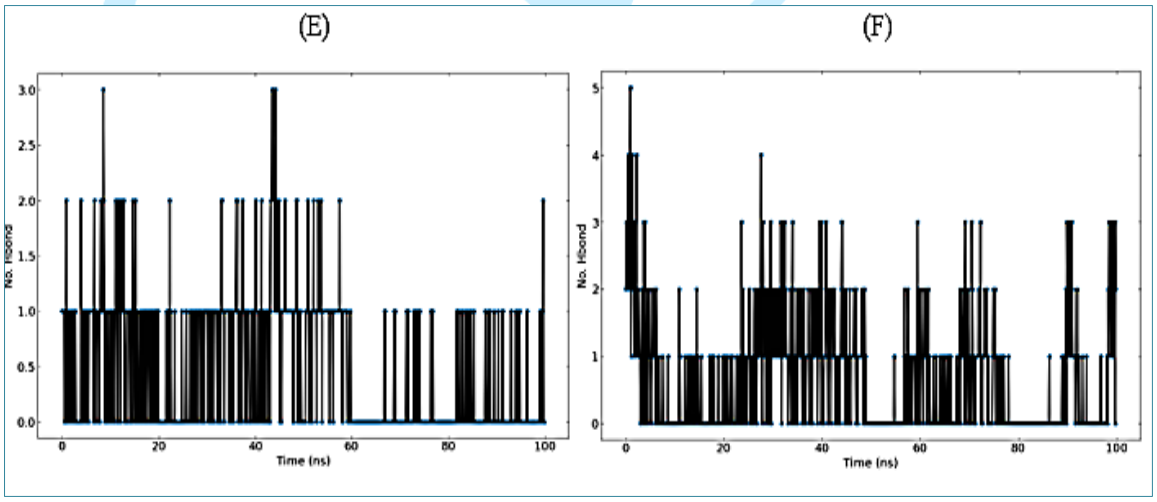

Fig. 13 Graphical representation of the number of H-bond contacts formed by the protein with the active molecule 2 (E), and the designed molecule M_1 (F)

3.9 Retrosynthesis analysis

Using the ASKCOS program, a retrosynthesis study was conducted on M1, the newly proposed most active molecule. Additionally, the interactive path planning module was utilized to determine if synthesizing the proposed new molecule was feasible. According to the results, the target molecule can be synthesized using this module in one step, giving five different pathways **Fig. 14,** ranked in descending order of plausibility from 100 % for the first two pathways to 98 % and 97 % for the other three reactions. In order to clarify the retrosynthesis pathways already proposed by the one-step module, this program has detailed the reactions, specifying the experimental conditions required to carry them out, such as reagents, solvents, temperature, and catalyst if necessary. In order to achieve our goal, the second reaction was considered an example since it has a 100% feasibility rate. We have identified the two essential reagents required to obtain M1 (as shown in

Fig. 15). ASKCOS has suggested ten ideal conditions for this reaction by altering one or more conditions, and the outcomes are listed in the **Table 8**. According to the results, the desired target represents the main product with a percentage of 93.14%, with some expected impurities presenting a percentage lower than 7%, showing high confidence in the proposed conditions **Fig.16**.

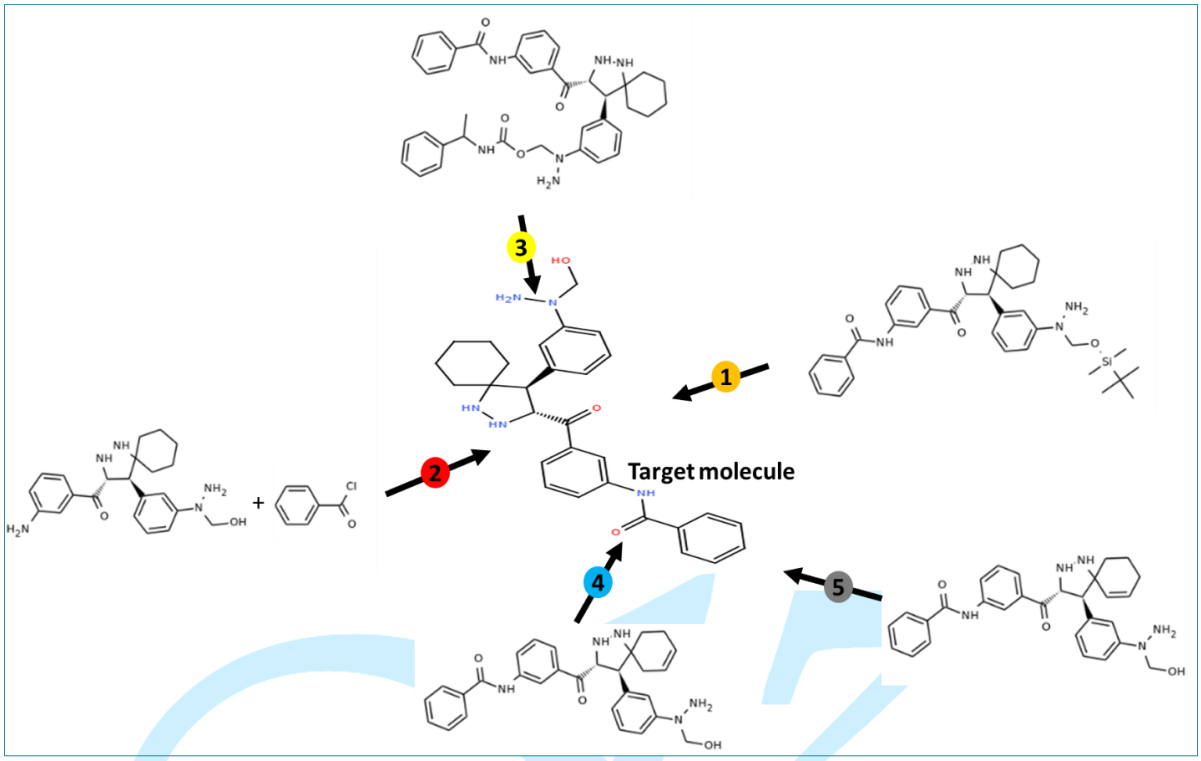

Fig. 14 One-step retrosynthesis prediction results for M1 molecule using the interactive path planning module implemented in ASKCOS

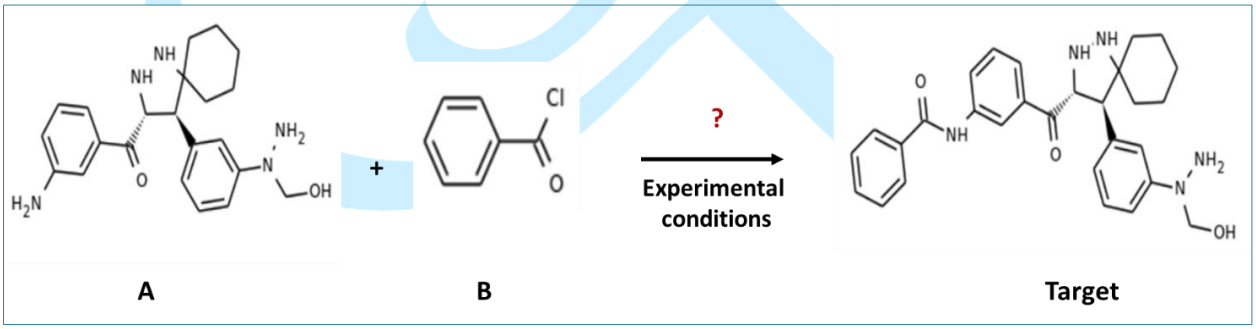

Fig. 15 Basic reagents for reaction two

Table 8 Ten best experimental conditions recommended for reaction 3

Rang	reagent	catalyst	Solvent	Temperature
1	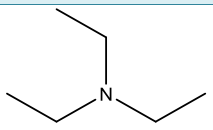	None	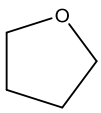	18°C
2	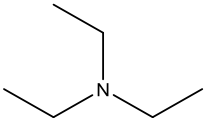	None	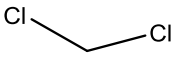	14°C
3	None	None	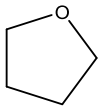	20°C

4	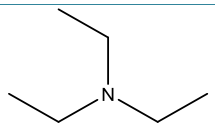	None	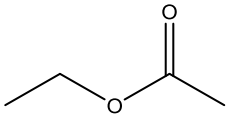	18°C
5	None	None	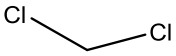	16°C
6	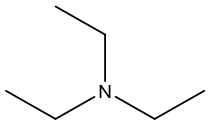	None	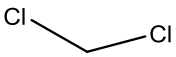	15°C
7	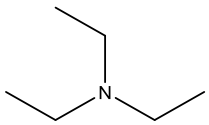	None	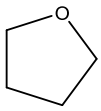	19°C
8	None	None	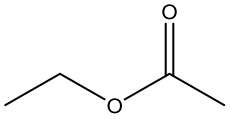	24°C
9	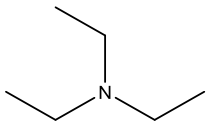	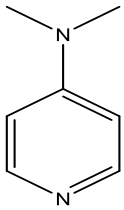	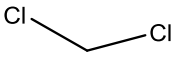	17°C
10	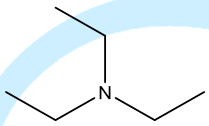	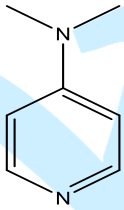	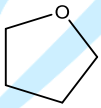	20°C

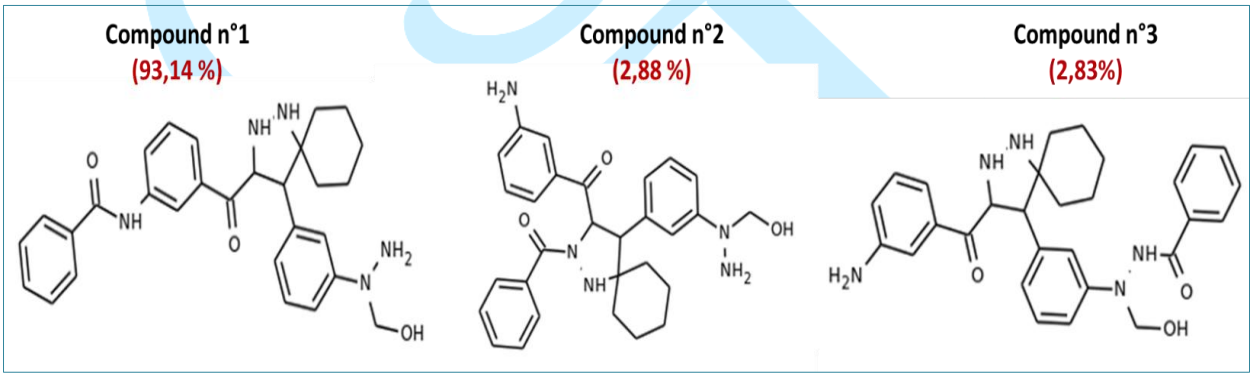

Fig. 16 Determination of the main product and impurities under the most recommended conditions

4. Conclusion

The research presents and discusses the computational studies (3D-QSAR, molecular docking, MD simulation, and ADMET prediction) of a series of spiropyrazoline derivatives as potential AD drugs. The (COMSIA/S + E + H) has high predictability and accuracy (Q2 = 0.517, R2 = 0.904, R2 test = 0.931). The obtained contour maps identified the relationship between the structure and activity of proposed spiropyrazoline derivatives as potential inhibitors, allowing an accurate prediction of the biochemical activity. The contour map results, including bulky substituents, hydrophobic groups, and highly electronegative atoms of R subsisting in Para position, can be beneficial in increasing the biological activity of spiropyrazoline derivatives. Molecular docking simulations also showed that the proposed M1 complex interacts with key residues on the main chain of AChE that are part of large circuits. The MD simulation verified the molecular docking results. According to Lipinski rule and ADMET profiling, the proposed spiropyrazoline derivatives have good absorption,

distribution, metabolism, and excretion properties. The proposed spiropyrazoline derivatives can be used as pharmacokinetic indicators to obtain more compounds for clinical trials. Finally, an efficient and practical synthetic route has been proposed to prepare the target molecule M1 using a retrosynthetic approach that simplifies the synthetic problem by identifying the main steps and reactions required to obtain the desired molecule by acting reversibly from the target molecule to the starting reactants.

Acknowledgements

We are grateful to the 'Association Marocaine des Chimistes Théoriciens' (AMCT) for its pertinent help concerning the programmes.

Funding Information

The authors did not receive any specific grant from funding agencies in the public, commercial, or not-for-profit sectors.

Declaration of Conflict

The authors declare that they have no known competing financial interests or personal relationships that could have appeared to influence the work reported in this paper.

References

1. Ali Mohammed Al-Ahmed, Z. (2022). Novel Cr(III), Ni(II), and Zn(II) complexes of thiocarbamide derivative: Synthesis, investigation, theoretical, catalytic, potentiometric, molecular docking and biological studies. *Arabian Journal of Chemistry*, *15*(9), 104104. https://doi.org/10.1016/j.arabjc.2022.104104
2. Coley, C. W., Thomas, D. A., Lummiss, J. A. M., Jaworski, J. N., Breen, C. P., Schultz, V., Hart, T., Fishman, J. S., Rogers, L., Gao, H., Hicklin, R. W., Plehiers, P. P., Byington, J., Piotti, J. S., Green, W. H., Hart, A. J., Jamison, T. F., & Jensen, K. F. (2019). A robotic platform for flow synthesis of organic compounds informed by AI planning. *Science*, *365*(6453), eaax1566. https://doi.org/10.1126/science.aax1566
3. Daina, A., Michielin, O., & Zoete, V. (2017). SwissADME: A free web tool to evaluate pharmacokinetics, drug-likeness and medicinal chemistry friendliness of small molecules. *Scientific Reports*, *7*, 42717. https://doi.org/10.1038/srep42717
4. De Strooper, B., & Karran, E. (2016). The cellular phase of Alzheimer's disease. *Cell*, *164*(4), 603–615. https://doi.org/10.1016/j.cell.2015.12.056
5. Dilshad, R., Khan, K.-R., Ahmad, S., Aati, H. Y., Al-Qahtani, J. H., Sherif, A. E., Hussain, M., Ghalloo, B. A., Tahir, H., Basit, A., & Ahmed, M. (2022). Phytochemical profiling, in vitro biological activities, and in-silico molecular docking studies of Typha domingensis. *Arabian Journal of Chemistry*, *15*(10), 104133. https://doi.org/10.1016/j.arabjc.2022.104133
6. El-Assaly, S. A., Ismail, A. E.-H. A., Bary, H. A., & Abouelenein, M. G. (2021). Synthesis, molecular docking studies, and antimicrobial evaluation of pyrano[2, 3-c]pyrazole derivatives. 10.5267/j.ccl, *309–328*. https://doi.org/10.5267/j.ccl.2021.3.003
7. Grest, G. S., & Kremer, K. (1986). Molecular dynamics simulation for polymers in the presence of a heat bath. *Physical Review. A, General Physics*, *33*(5), 3628–3631. https://doi.org/10.1103/PhysRevA.33.3628
8. Gutti, G., Kumar, D., Paliwal, P., Ganeshpurkar, A., Lahre, K., Kumar, A., Krishnamurthy, S., & Singh, S. K. (2019). Development of pyrazole and spiropyrazoline analogs as multifunctional agents for treatment of Alzheimer's disease. *Bioorganic Chemistry*, *90*, 103080. https://doi.org/10.1016/j.bioorg.2019.103080
9. Islam, N., Islam, M. D., Rahman, Md. R., & Matin, M. M. (2021). Octyl 6-O-hexanoyl-β-D-glucopyranosides: Synthesis, PASS, antibacterial, in silico ADMET, and DFT studies. *Current Chemistry Letters*, *10*(4), 413–426. https://doi.org/10.5267/j.ccl.2021.5.003

10. Kareti, S. R., & Subash, P. (2020). In silico exploration of anti-Alzheimer's compounds present in methanolic extract of Neolamarckia Cadamba bark using GC–MS/MS. *Arabian Journal of Chemistry*, *13*(7), 6246–6255. https://doi.org/10.1016/j.arabjc.2020.05.035
11. Khalil, A., El-Khouly, A. S., Elkaeed, E. B., & Eissa, I. H. (2022). The Inhibitory Potential of 2'-dihalo Ribonucleotides against HCV: Molecular Docking, Molecular Simulations, MM-BPSA, and DFT Studies. *Molecules*, *27*(14), 4530. https://doi.org/10.3390/molecules27144530
12. Khedkar, V. M., Ambre, P. K., Verma, J., Shaikh, M. S., Pissurlenkar, R. R. S., & Coutinho, E. C. (2010a). Molecular docking and 3D-QSAR studies of HIV-1 protease inhibitors. *Journal of Molecular Modeling*, *16*(7), 1251–1268. https://doi.org/10.1007/s00894-009-0636-5
13. Khedkar, V. M., Ambre, P. K., Verma, J., Shaikh, M. S., Pissurlenkar, R. R. S., & Coutinho, E. C. (2010c). Molecular docking and 3D-QSAR studies of HIV-1 protease inhibitors. *Journal of Molecular Modeling*, *16*(7), 1251–1268. https://doi.org/10.1007/s00894-009-0636-5
14. Li, X., Ye, L., Shi, W., Liu, H., Liu, C., Qian, X., Zhu, Y., & Yu, H. (2013). In silico study on hydroxylated polychlorinated biphenyls as androgen receptor antagonists. *Ecotoxicology and Environmental Safety*, *92*, 258–264. https://doi.org/10.1016/j.ecoenv.2013.03.008
15. Liu, J. Z., Lyu, H. C., Fu, Y. J., & Cui, Q. (2022). Amomum tsao-ko essential oil, a novel anti-COVID-19 Omicron spike protein natural products: A computational study. *Arabian Journal of Chemistry*, *15*(7), 103916. https://doi.org/10.1016/j.arabjc.2022.103916
16. Liu, Y., Grimm, M., Dai, W. T., Hou, M. C., Xiao, Z. X., & Cao, Y. (2020). CB-Dock: A web server for cavity detection-guided protein–ligand blind docking. *Acta Pharmacologica Sinica*, *41*(1), 138–144. https://doi.org/10.1038/s41401-019-0228-6
17. Long, J. M., & Holtzman, D. M. (2019). Alzheimer disease: An update on pathobiology and treatment strategies. *Cell*, *179*(2), 312–339. https://doi.org/10.1016/j.cell.2019.09.001
18. Meng, X., Cui, L., Song, F., Luan, M., Ji, J., Si, H., Duan, Y., & Zhai, H. (2020). 3D-QSAR and molecular docking studies on design anti-prostate cancer curcumin analogues. *Current Computer-Aided Drug Design*, *16*(3), 245–256. https://doi.org/10.2174/1573409914666181029123746
19. O'Boyle, N. M., Banck, M., James, C. A., Morley, C., Vandermeersch, T., & Hutchison, G. R. (2011). Open Babel: An open chemical toolbox. *Journal of Cheminformatics*, *3*, 33. https://doi.org/10.1186/1758-2946-3-33
20. Phillips, J. C., Braun, R., Wang, W., Gumbart, J., Tajkhorshid, E., Villa, E., Chipot, C., Skeel, R. D., Kalé, L., & Schulten, K. (2005). Scalable molecular dynamics with NAMD. *Journal of Computational Chemistry*, *26*(16), 1781–1802. https://doi.org/10.1002/jcc.20289
21. Pires, D. E. V., Blundell, T. L., & Ascher, D. B. (2015). pkCSM: Predicting small-molecule pharmacokinetic and toxicity properties using graph-based signatures. *Journal of Medicinal Chemistry*, *58*(9), 4066–4072. https://doi.org/10.1021/acs.jmedchem.5b00104
22. Ponce, L. F., Ramirez-Echemendia, D. P., Leon, K., & Valiente, P. A. (2021). Deciphering PD1 activation mechanism from molecular docking and molecular dynamic simulations [Preprint]. *Bioinformatics*. https://doi.org/10.1101/2021.09.16.460652
23. Rapaport, D. C., Blumberg, R. L., McKay, S. R., & Christian, W. (1996). The art of Molecular Dynamics simulation. *Computers in Physics*, *10*(5), 456. https://doi.org/10.1063/1.4822471
24. Rose, A. S., Bradley, A. R., Valasatava, Y., Duarte, J. M., Prlić, A., & Rose, P. W. (2018). NGL viewer: Web-based molecular graphics for large complexes. *Bioinformatics*, *34*(21), 3755–3758. https://doi.org/10.1093/bioinformatics/bty419
25. Shen, Y., Borowski, J. E., Hardy, M. A., Sarpong, R., Doyle, A. G., & Cernak, T. (2021). Automation and computer-assisted planning for chemical synthesis. *Nature Reviews Methods Primers*, *1*(1), 23. https://doi.org/10.1038/s43586-021-00022-5
26. Srivastava, V., Gupta, S. P., Siddiqi, M. I., & Mishra, B. N. (2010). 3D-QSAR studies on quinazoline antifolate thymidylate synthase inhibitors by CoMFA and CoMSIA models. *European Journal of Medicinal Chemistry*, *45*(4), 1560–1571. https://doi.org/10.1016/j.ejmech.2009.12.065

27. Tanenbaum, D. R., & Lark, M. R. (2022). Masticatory/temporomandibular disorders: Practical Assessment and Care Concepts for the Otolaryngologist. *Otolaryngologic Clinics of North America*, *55*(3), 659–679. https://doi.org/10.1016/j.otc.2022.02.012
28. Vyas, N. A., Singh, S. B., Kumbhar, A. S., Ranade, D. S., Walke, G. R., Kulkarni, P. P., Jani, V., Sonavane, U. B., Joshi, R. R., & Rapole, S. (2018). Acetylcholinesterase and Aβ aggregation inhibition by heterometallic ruthenium(II)−platinum(II) polypyridyl complexes. *Inorganic Chemistry*, *57*(13), 7524–7535. https://doi.org/10.1021/acs.inorgchem.8b00091
29. Yao, M., Nie, H., Yao, W., Yang, X., & Zhang, G. (2022). A sensitive and selective fluorescent probe for acetylcholinesterase: Synthesis, performance, mechanism and application. *Arabian Journal of Chemistry*, *15*(7), 103929. https://doi.org/10.1016/j.arabjc.2022.103929
30. Yu, N., Xuan Quan, W., Li Li, J., Shu, M., Wang, R., Shen, Y., Hua Lin, Z., & Ying Sun, J. (2022). 3D-QSAR, molecular docking and Molecular Dynamics analysis of 1,2,3,4-Tetrahydroquinoxalines as BRD4/BD2 inhibitors. *ChemistrySelect*, *7*(18). https://doi.org/10.1002/slct.202200442
31. Yu, X., Zhao, X., Zhang, Q., Dai, C., Huang, Q., Zhang, L., Liu, Y., Shen, Y., & Lin, Z. (2023). Discovery of neuraminidase Inhibitors based on 3D-QSAR, Molecular Docking and MD Simulations. *ChemistrySelect*, *8*(12), e202203978. https://doi.org/10.1002/slct.202203978
32. Zeng, G. H., Fang, D. Q., Wu, W. J., Zhang, R., Xie, W. G., Wu, J. H., & Shen, Y. (2013). Binding conformations, QSAR, and molecular design of Alkene-3-quinolinecarbonitriles as Src inhibitors. *International Journal of Quantum Chemistry*, *113*(10), 1467–1478. https://doi.org/10.1002/qua.24344